Water Resources Research®

Potential Evaporation and the Complementary Relationship

Zhuoyi Tu[1], Yuting Yang[1] , Michael L. Roderick[2] , and Tim R. McVicar[3]

[1]State Key Laboratory of Hydroscience and Engineering, Department of Hydraulic Engineering, Tsinghua University, Beijing, China, [2]Research School of Earth Sciences, Australian National University, Canberra, ACT, Australia, [3]CSIRO Environment, Canberra, ACT, Australia

Abstract The complementary relationship (CR) provides a framework for estimating land surface evaporation with basic meteorological observations by acknowledging the relationship between actual evaporation, apparent potential evaporation and potential evaporation (E_{po}). As a key variable in the CR, E_{po} estimates by conventional models have a long-standing problem in practical applications. That is, the meteorological forcings (i.e., radiation and temperature) employed in conventional E_{po} models are observed under actual conditions that are generally not saturated. Hence, conventional E_{po} models do not conform to the original definition of E_{po} (i.e., the evaporation that would occur with an unlimited water supply). Here, we estimate E_{po} using the maximum evaporation approach (E_{po_max}) that does follow the original E_{po} definition. We find that adopting E_{po_max} considerably reduces the asymmetry of the CR compared to when the conventional Priestley-Taylor E_{po} is used. We then employ E_{po_max} and develop a new physically based, calibration-free CR model, which shows an overall good performance in estimating actual evaporation in 705 catchments at the mean annual scale and 64 flux sites at monthly and mean annual scales (R^2 ranges from 0.73 to 0.75 and root-mean-squared error ranges from 9.8 to 18.8 W m^{-2}). Both the 705 catchments and 64 flux sites cover a wide range of climates. More importantly, the use of E_{po_max} leads to a new physical interpretation of the CR.

1. Introduction

Terrestrial evaporation (E) is a crucial linkage between water, energy and carbon cycles (Green et al., 2019; Oki & Kanae, 2006; Trenberth et al., 2009). Given this importance, various methods have been developed to estimate E (Brutsaert, 1982, 2005; McMahon et al., 2013; K. Wang & Dickinson, 2012). Among them, the complementary relationship (CR; Bouchet, 1963) provides a framework for estimating E with basic meteorological observations based on a hypothesized relationship between E, apparent potential evaporation (E_{pa}) and potential evaporation (E_{po}) of the form,

$$E = f\left(E_{pa}, E_{po}\right) \tag{1}$$

in which E_{pa} is the evaporation from a small wet surface located in the same drying environment as where E takes place, and E_{po} is the evaporation that occurs from the same large surface as E when the underlying surface is non-water-limited and with the same solar radiative input (Brutsaert, 2015). The physical interpretation of the CR is that as the land surface gets wetter, E becomes larger due to increased water supply. Thus the increasing E (latent heat flux) and decreasing sensible heat flux (H) make the air passing over the surface wetter and cooler (increasing specific humidity q and decreasing air temperature T_a) with E_{pa} becoming smaller as the vapor pressure deficit (VPD) decreases (Figure 1; Morton, 1983). When the underlying surface becomes saturated, the difference between E and E_{pa} diminishes and both approach E_{po} (Figure 1). As first postulated by Bouchet (1963), the original symmetric linear relationship proposed that E and E_{pa} depart from E_{po} with equal yet opposite changes (Bouchet, 1963; Brutsaert & Stricker, 1979; Morton, 1983). However, this strict symmetric CR has not been found in observations and has instead evolved into an asymmetric linear relationship (Brutsaert & Parlange, 1998; Granger, 1989; Kahler & Brutsaert, 2006; Szilagyi, 2007). More recently, a new generalized nonlinear CR (Brutsaert, 2015; S. Han & Tian, 2018; Szilagyi et al., 2017) has received increasing attention and offers opportunities for estimating E (e.g., Brutsaert et al., 2020; S. Han & Tian, 2020; Ma et al., 2021).

As key variables in the CR, the definitions of E_{pa} and E_{po} have been widely debated (Aminzadeh et al., 2016; Brutsaert & Stricker, 1979; Granger, 1989; S. Han & Tian, 2020; Morton, 1983). Most studies suggest that E_{pa} can be estimated with pan evaporation or calculated using the Penman (1948) equation (e.g., Brutsaert, 2015;
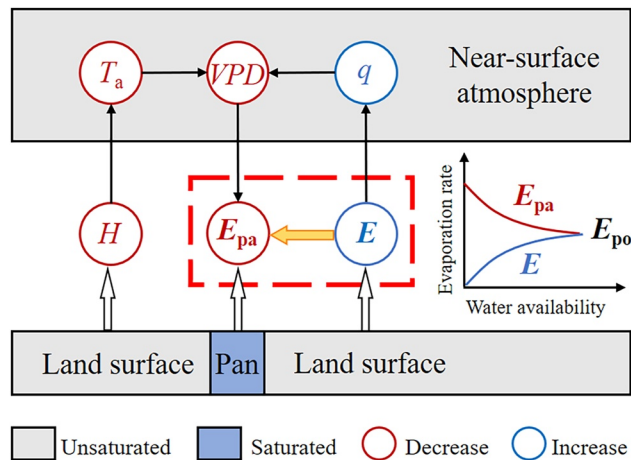
Figure 1. The conceptual basis of the complementary relationship. When the surface becomes wetter, E increases and H decreases due to more water supply, resulting in a cooler and moister (decreasing T_a and increasing q) near-surface atmosphere. This further leads to a reduction in VPD, which decreases E_{pa}. Based on this principle, the complementary relationship describes the relationship between the increasing E and decreasing E_{pa} as the water supply increases. All symbols are defined in the text.

Brutsaert & Stricker, 1979; J. Han et al., 2020; Szilagyi et al., 2017; L. Zhang & Brutsaert, 2021). However, the calculation of E_{po} has a long-standing problem conflicting with its physical definition. In theory, E_{po} is the evaporation when the surface is non-water-stressed and should be calculated by using meteorological variables (e.g., radiation, temperature) corresponding to a hypothetical saturated surface. In practice, the conventional E_{po} models (e.g., the most widely used is the Priestley and Taylor (1972) model) employ the meteorological variables observed over real surfaces that are generally not saturated, contradicting the E_{po} definition. Compared with the hypothetical wet conditions, the observed higher temperature and lower net radiation under non-saturated conditions would result in an underestimation of E_{po} using the Priestley-Taylor model (Tu & Yang, 2022), which hinders a correct understanding and interpretation of the CR.

The issue that conventional E_{po} calculations do not conform to the potential conditions has been widely recognized by the CR research community (S. Han & Tian, 2020; Szilagyi et al., 2017; L. Zhang & Brutsaert, 2021). However, mainstream generalized CR formulations still suffer from the above "potential" problems (i.e., employing the meteorological variables observed under real conditions that are usually not saturated) in E_{po} calculation. For example, in the generalized polynomial CR model proposed by Brutsaert (2015), E_{po} is calculated by multiplying the equilibrium evaporation (E_{rad}) with a fitted coefficient (i.e., α). By calibrating the model with observed E, α is determined to have a value lower than 1 in many parts of the world, especially in relatively dry regions (Brutsaert et al., 2020; X. Liu et al., 2016; L. Zhang et al., 2017). This is physically unrealistic, as E_{rad} sets the lower limit of E_{po} (Philip, 1987). This suggests that there is an internal inconsistency in Brutsaert's generalized polynomial CR model. To address this issue, Szilagyi et al. (2017) proposed a calibration-free CR formulation, where α is a fixed value estimated with data over extensive wet areas (around 1.10; Ma et al., 2019, 2021; Szilagyi et al., 2017). In addition, they also realized that the observed T_a does not correspond to the temperature under non-water-stressed conditions in calculating E_{po} and handled this issue by estimating a wet surface temperature (T_{ws}). In their approach, T_{ws} is derived by equating the Bowen ratio of an extensive wet surface to that of a plot-size wet surface (Szilagyi & Jozsa, 2008), with the assumption of constant net radiation (R_n) under both wet and dry conditions. Nevertheless, R_n is always a function of surface temperature according to Stefan-Boltzmann's law (Monteith, 1981), so R_n and T_s are physically interdependent. Tu and Yang (2022) demonstrated that merely using T_{ws} (e.g., R. D. Crago & Qualls, 2021; Qualls & Crago, 2020; Szilagyi, 2014, 2021; Szilagyi & Schepers, 2014; Szilagyi et al., 2017, 2022) and ignoring the R_n dependence of T_s would result in an even lower E_{po} estimate (compared to the conventional Priestley-Taylor model). To avoid the difficulties in formulating E_{po}, the generalized sigmoid CR formulation (S. Han & Tian, 2018; S. Han et al., 2012) abandons the concept of E_{pa} and E_{po} and uses Penman's potential evaporation (E_{Pen}) and its radiative component (equivalent to E_{rad}) to describe the relationships with E. However, this sigmoid CR deviates from the fundamental complementarity between E, E_{pa}, and E_{po} and has a vague physical interpretation. Moreover, an additional parameter that requires local calibration is introduced into that model for practical application in estimating E, which prevents the application of that model over regions without prior knowledge of E. To sum up, despite all the efforts, estimation of E_{po} is still a general and fundamental issue in the state-of-the-art CR models. This issue prevents a proper interpretation of the CR and as importantly, hinders further developments of the CR.

Recently, Yang and Roderick (2019) developed a maximum evaporation method that explicitly acknowledges the interactions between evaporation, surface temperature (T_s) and radiation over saturated surfaces. This new approach calculates the net longwave radiation and T_s for a large hypothetical saturated surface (Tu et al., 2022; Yang & Roderick, 2019). In a following study, Tu and Yang (2022) demonstrated that the maximum evaporation corresponds to E_{po}. In more detail, E_{po} is consistent with the fundamental definition of potential evaporation as the evaporation that takes place from the same surface as the actual evaporation when the available water is not a limiting factor and with the same solar radiative input (Brutsaert, 2015). With that, the main objectives of this study are to (a) investigate the CR with E_{po} estimated using the maximum evaporation method, and (b) develop a new, physically based, calibration-free CR model for estimating actual evaporation. In the following text, the data sets used in the
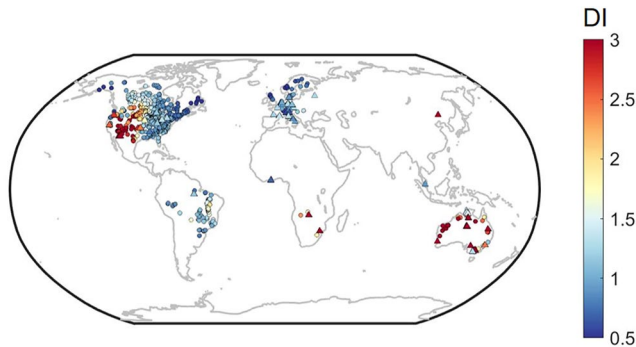
Figure 2. Locations of the 705 catchments (circles) and the 64 flux sites (triangles) used in this study. Colors represent the dryness index (DI).

study are described in Section 2. In Section 3, we will briefly introduce the maximum evaporation method and investigate the implications of using E_{po} from the maximum evaporation approach in the CR. Conventional E_{po} estimates based on the Priestley-Taylor model will also be adopted for comparison. In Section 4, a physically based and calibration-free CR formulation employing E_{po} calculated from the maximum evaporation method will be developed. This new CR formulation will be evaluated across catchments at the mean annual scale and across flux sites at both monthly and mean annual scales. Discussion and conclusions will be made in Section 5 and 6, respectively.

2. Data Sets

2.1. Data for Catchments

For the model forcings, monthly meteorological variables (i.e., near-surface air temperature, specific humidity, air pressure, wind speed, and precipitation) and radiative fluxes (i.e., incoming and net shortwave radiation, incoming and net longwave radiation, incoming shortwave radiation at the top of the atmosphere) at a spatial resolution of 0.25° from 1982 to 2011 were obtained from the ERA5 global reanalysis data set (https://doi.org/10.24381/cds.f17050d7; Hersbach et al., 2020).

Continuous daily or monthly streamflow (Q) observations from 1982 to 2011 in 994 unimpaired catchments (all larger than 2,500 km^2) were collected from a recent study by J. Han et al. (2020). These 994 catchments were chosen from a more comprehensive collection of more than 22,000 catchments globally (Beck et al., 2020; Yang et al., 2021) and all have a negligible water storage change at the 30-year scale so the mean annual E can be safely estimated as the difference between mean annual precipitation (obtained from ERA5 data set) and mean annual Q (see J. Han et al. (2020) for details). Additionally, catchments near seashores (less than 200 km from the coastline) are removed to avoid strong land-sea advection effects (Ma et al., 2021) as the coupling of the land-atmosphere system weakens substantially near sudden jumps of wetness conditions (Morton, 1983; Szilagyi, 2021). This additional criterion excluded 289 catchments and the remaining 705 catchments were used in the following analyses. Figure 2 shows the spatial distribution of the 705 catchments and their dryness index (DI, defined as E_{pa}/P at the mean annual scale).

2.2. Eddy-Covariance Data From FLUXNET2015

Observations of monthly actual evaporation (or latent heat flux) along with relevant meteorological variables and radiative fluxes were also obtained from 64 flux sites within the FLUXNET2015 database (http://fluxnet.fluxdata.org/data/fluxnet2015-dataset/; Pastorello et al., 2020) (Figure 2, Table S1 in Supporting Information S1). The monthly variables were derived based on half-hourly observations at each site. Only months with the data quality metric for latent heat flux and radiative fluxes higher than 0.9 (on a scale of 0–1 provided by FLUXNET) were retained. The 64 sites were selected based on the following three criteria, including (a) the site existed for at least 3 years; (b) the site has at least 12 months of data after quality check; and (c) the site is away from the coastline. Finally, the flux data were adjusted to ensure energy budget closure using the residual approach, which assumes the observed sensible heat flux is correct and considers latent heat flux as the residual of the surface energy balance equation (Ershadi et al., 2014).

3. Estimations of E_{po} and the Implications for the Complementary Relationships

3.1. Formulations of E_{pa} and E_{po} in the Complementary Relationship

As key variables in the CR, E_{pa} and E_{po} need to be determined. Defined by Brutsaert (2015), E_{pa} is the evaporation from a small wet surface, located in the same environment and surrounded by the drying surface where E is occurring. This means that E_{pa} can be determined with pan evaporation or estimated from the Penman (1948) equation,

$$E_{pa} = \frac{\Delta}{\Delta + \gamma}(R_n - G) + \frac{\gamma}{\Delta + \gamma} f_e(u_2)(e_s - e_a) \qquad (2)$$

where R_n is the net radiation (W m^{-2}), G is the ground heat flux (W m^{-2}) and is often ignored over land for the time scales longer than a day over terrestrial surfaces (Shuttleworth, 1993), γ is the psychrometric constant (kPa K^{-1}), Δ is the slope of the saturation vapor pressure curve (kPa K^{-1}), e_a is the vapor pressure (hPa) and e_s (hPa) denotes saturation vapor pressure. The variable u_2 is the wind speed measured at 2 m height, and $f_e(u_2)$ (mm day^{-1} hPa^{-1}) is an empirical wind function (Brutsaert, 1982),

$$f_e(u_2) = 0.26(1 + 0.54u_2) \tag{3}$$

Different from E_{pa}, E_{po} is defined as the evaporation that occurs from the same large-size surface of E when the evaporating water is not a limiting factor. Here, we adopt the maximum evaporation approach, which is able to recover radiation and temperature to a (hypothetical) wet condition, to estimate E_{po} (Tu et al., 2022; Yang & Roderick, 2019). Tu and Yang (2022) demonstrated that E_{po} estimated from the maximum evaporation approach follows the E_{po} definition. The maximum evaporation method calculates evaporation as,

$$E_{po\_max} = \frac{R_n(T_s) - G}{1 + \beta(T_s)} \tag{4}$$

where β is the Bowen ratio, defined as the ratio of sensible heat flux (H) over latent heat flux (i.e., $\beta = H/LE$) and T_s (K) is the temperature at the evaporating surface.

To explicitly acknowledge the dependence of R_n on T_s, R_n is estimated as (Yang & Roderick, 2019),

$$R_n(T_s) = R_{sn} + \varepsilon\sigma(T_s - \Delta T)^4 - \varepsilon\sigma T_s^{\ 4} \tag{5}$$

where R_{sn} is the observed net shortwave radiation (W m^{-2}), ε is the surface emissivity and σ is the Stefan-Boltzmann constant (5.67×10^{-8} W m^{-2} K^{-4}). ΔT is the temperature difference between T_s and the effective radiating temperature of the atmosphere and is parameterized as a function of shortwave atmospheric transmissivity (τ; the ratio of incoming shortwave radiation at the Earth's surface over incoming shortwave radiation at the top of the atmosphere) and geographic latitude (lat),

$$\Delta T = n_1 \exp(n_2\tau) + n_3|\text{lat}| \tag{6}$$

where n_1, n_2, and n_3 are fitting coefficients. Here, we quantify these three coefficients (i.e., $n_1 = 1.28$, $n_2 = 3.72$, and $n_3 = 0.083$; also see Figure S1 in Supporting Information S1) using relevant data from ERA5 under wet conditions. The grid-boxes/months at which evaporation is not limited by water stress (i.e., wet condition) over land are determined following Milly and Dunne (2016) and Yang et al. (2019).

The Bowen ratio (β) is expressed as a function of T_s,

$$\beta(T_s) = m_1 \frac{\gamma(T_s)}{\Delta(T_s)} + m_2 \tag{7}$$

where m_1 and m_2 are fitting coefficients. We adopt the value of $m_1 = 0.24$ and $m_2 = 0$ determined over global ocean surfaces following Yang and Roderick (2019). These two values are also consistent with those determined over global wetlands (Tu et al., 2022).

In Equation 4, both R_n and β vary inversely with T_s, implying a maximum evaporation along the T_s gradient that has been previously assessed as consistent with the actual evaporation over wet surfaces (Tu et al., 2022; Yang & Roderick, 2019). To apply the maximum evaporation method, an array of T_s (e.g., from 250 to 330 K at an interval of 0.1 K) along with the observed R_{sn} are applied to Equations 5 and 7 and then Equation 4 to estimate evaporation at the corresponding T_s. The maximum evaporation along the T_s gradient is chosen as the potential evaporation over a hypothetical large saturated surface.

In addition, we also calculate E_{po} using the Priestley and Taylor (1972) model for comparison, which is the most widely used E_{po} model in existing CR models. The Priestley-Taylor model estimates E_{po} as,

$$E_{po\_PT} = \alpha \frac{\Delta}{\Delta + \gamma}(R_n - G) \tag{8}$$

where α is the Priestley-Taylor coefficient, which was originally determined to be 1.26 (Priestley & Taylor, 1972).
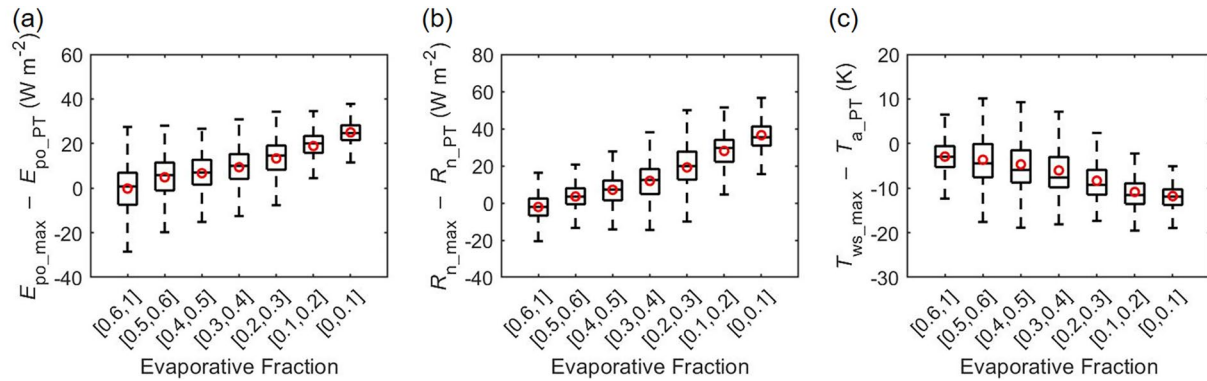
Figure 3. Difference between (a) E_{po_max} and E_{po_PT}, (b) R_{n_max} and R_{n_PT}, and (c) T_{ws_max} and T_{a_PT}, along a moisture gradient (as indicated by the evaporative fraction) across the 705 catchments and 64 flux sites.

3.2. Complementary Relationships With Different E_{po} Calculations

In this section, we first compare the two E_{po} estimates and examine the implications of different E_{po} estimates in the CR with monthly grided ERA5 forcing data in 705 catchments and observed data at 64 flux sites.

Figure 3a shows the difference between monthly E_{po} estimates from the maximum evaporation method (E_{po_max}) and the Priestley-Taylor model (E_{po_PT}) along a moisture gradient (as indicated by the evaporative fraction, $EF = LE/(R_n - G)$). The results show that E_{po} estimates from these two models are very close under wet conditions (i.e., $EF > 0.6$) but the difference between E_{po_max} and E_{po_PT} becomes increasingly larger as the surface gets drier (i.e., lower EF). Under extremely dry conditions (e.g., $EF < 0.1$), E_{po_max} is typically 20 W m^{-2} (~260 mm yr^{-1}) higher than E_{po_PT}. The higher E_{po_max} than E_{po_PT} under dry conditions is primarily caused by a higher R_n when recovered to a hypothetical wet surface in the maximum evaporation approach (R_{n_max}) compared to the ERA5 R_n under actual conditions that is directly adopted by the Priestley-Taylor model (R_{n_PT}; Figure 3b) and a lower wet surface temperature in the maximum evaporation approach (T_{ws_max}) than the ERA5 T_a under actual conditions used by the Priestley-Taylor model (T_{a_PT}; Figure 3c). In summary, our results show that R_{n_max} and T_{ws_max} estimated from the maximum evaporation method essentially follow R_{n_PT} and T_{a_PT} when the surface is wet. However, as the surface becomes drier, R_{n_max} is increasingly larger than R_{n_PT} and T_{ws_max} is increasingly smaller than T_{a_PT}, with the difference in net radiation (i.e., $R_{n\_max} - R_{n\_PT}$) approaching 40 W m^{-2} and that in temperature (i.e., $T_{a\_PT} - T_{ws\_max}$) exceeding 10 K when the underlying surface is severely water limited (Figures 3b and 3c). It should be noted that since the maximum evaporation method uses the observed net shortwave radiation, the difference between R_{n_max} and R_{n_PT} represents differences in the longwave components.

Figure 4 shows the CR for the 64 flux sites when different E_{po} estimates are used at the monthly scale. Since E_{po_max} is higher than E_{po_PT}, it is not surprising that E/E_{po_PT} and E_{pa}/E_{po_PT} are both higher than E/E_{po_max} and E_{pa}/E_{po_max}, especially under dry conditions (i.e., E/E_{pa} is low). The lower values of E/E_{po_max} and E_{pa}/E_{po_max} remarkably reduce the asymmetry of the CR and constrain the data points within much narrower ranges, compared with that when E_{po_PT} is used.
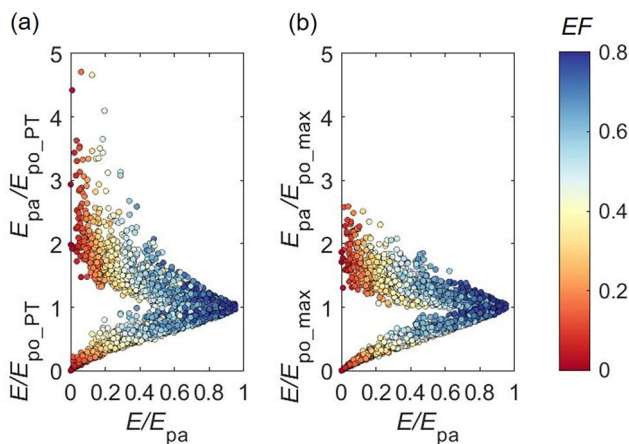

Figure 4. Illustration of the complementary relationships between the actual evaporation E and the apparent potential evaporation E_{pa}, scaled by different E_{po} estimates, along a moisture availability gradient (as expressed by the ratio of E/E_{pa}) with monthly flux data at the 64 flux sites. (a) E_{po} is estimated by the Priestley-Taylor model and (b) E_{po} is estimated by the maximum evaporation method. Colors represent the degree of wetness (as indicated by the evaporative fraction). In both subplots, dots larger than 1 on the Y-axis are E_{pa}/E_{po} and dots smaller than 1 on the Y-axis are E/E_{po}.

4. A Physically Based CR Model Adopting E_{po_max}

4.1. Model Development

The above results clearly show that using E_{po_max} that closely follows the definition of potential evaporation leads to a different CR compared with that when E_{po} is calculated from the conventional Priestley-Taylor model. In the following, we present the development of a new CR model for estimating actual evaporation, in which E_{po_max} is adopted for potential evaporation.

Following Brutsaert (2015), the three variables in the CR (i.e., E, E_{pa}, and E_{po}) can be reduced to two dimensionless variables, $x = E_{po}/E_{pa}$ and $y = E/E_{pa}$, subject to the following boundary conditions,

$$\begin{cases} y = 1 & \text{when} & x = 1 \\ y = 0 & \text{when} & x = 0 \\ dy/dx = 1 & \text{when} & x = 1 \\ dy/dx = 0 & \text{when} & x = 0 \end{cases} \tag{9}$$

Brutsaert (2015) originally introduced a polynomial function that satisfies the above four boundary conditions as,

$$y = 2x^2 - x^3 \tag{10}$$

Subsequent studies pointed out that the second boundary condition (i.e., $y = 0$, $x = 0$) only holds if either E_{pa} is infinitely large or E_{po} is zero when the underlying surface is extremely water-limited, both of which are physically unrealistic (R. Crago et al., 2016; Szilagyi et al., 2017). Szilagyi et al. (2017) dealt with this challenge by assuming there exists a maximum E_{pa} (E_{pa_max}) under extremely dry conditions and rescaled x to a new variable denoted X,

$$X = \frac{E_{pa\_max} - E_{pa}}{E_{pa\_max} - E_{po}} x = \frac{E_{pa\_max} - E_{pa}}{E_{pa\_max} - E_{po}} \frac{E_{po}}{E_{pa}} \tag{11}$$

Then, the revised complementary function is (Szilagyi et al., 2017),

$$y = 2X^2 - X^3 \tag{12}$$

The boundary conditions for Equation 12 are,

$$\begin{cases} y = 1 & \text{when} & X = 1 \\ y = 0 & \text{when} & X = 0 \\ dy/dX = 1 & \text{when} & X = 1 \\ dy/dX = 0 & \text{when} & X = 0 \end{cases} \tag{13}$$

According to Szilagyi et al. (2017), the value of E_{pa_max} (required in Equation 11) can be estimated by the Penman equation when the air reaches the driest conditions ($e_a = 0$),

$$E_{pa\_max} = \frac{\Delta(T_{a\_dry})}{\Delta(T_{a\_dry}) + \gamma} R_n + \frac{\gamma}{\Delta(T_{a\_dry}) + \gamma} f_e(u_2) e_s(T_{a\_dry}) \tag{14}$$

where T_{a_dry} (K) is the air temperature when e_a approaches 0 following an adiabatic process (Monteith, 1981),

$$T_{a\_dry} = T_a + e_a/\gamma \tag{15}$$

Two issues exist in the above processes of estimating E_{pa_max}. First, to determine T_{a_dry}, e_a is assumed to be zero. However, in real conditions, e_a hardly approaches zero even in the middle of a large dry desert, especially at relatively long time scales. Analysis of ERA5 monthly humidity data shows that the lowest single monthly relative humidity (RH) over 1982–2011 across the entire terrestrial surface is 4% and the 0.1th percentile of monthly RH is 10% (Figure S2 in Supporting Information S1). Second and more importantly, the above processes of estimating T_{a_dry} and E_{pa_max} ignore the intrinsic interdependence between temperature and radiation. More specifically, observed R_n under real conditions is used in the Penman model to estimate E_{pa_max} (Equation 14). This is incorrect, as when T_a approaches T_{a_dry}, R_n also changes in accordance with T_a and approaches the net radiation under (hypothetical) extremely dry conditions (i.e., R_{n_dry}).

To solve the above two problems, corresponding meteorological variables (i.e., e_a, T_a, and R_n) need to be restored to extremely dry conditions when estimating E_{pa_max},
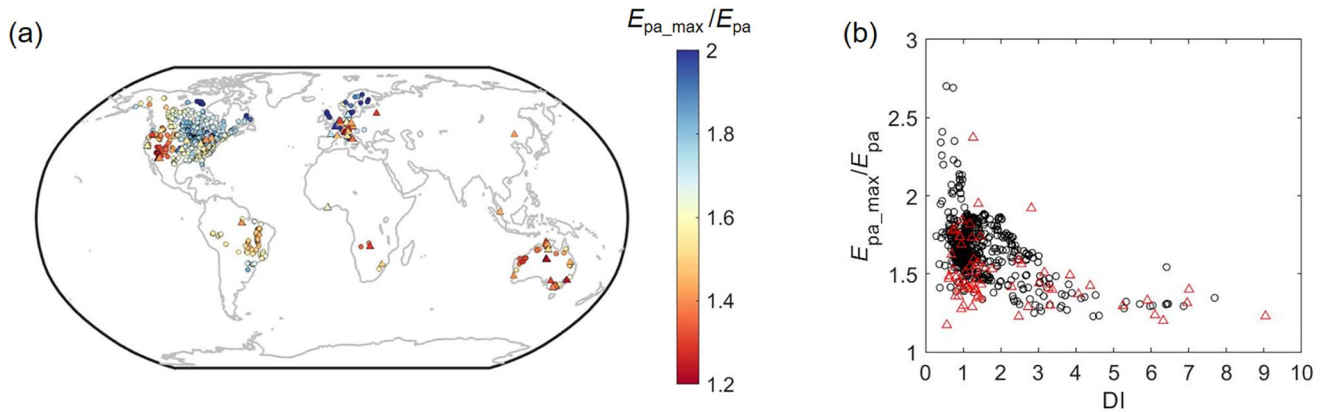
Figure 5. Distribution of the mean annual ratio of E_{pa_max} over E_{pa} at catchments (circle) and flux sites (triangle). (b) Relationship between the mean annual ratio of E_{pa_max} over E_{pa} and the dryness index (DI) at catchments (black circle) and flux sites (red triangle).

$$E_{pa\_max} = \frac{\Delta(T_{a\_dry})}{\Delta(T_{a\_dry}) + \gamma} R_{n\_dry} + \frac{\gamma}{\Delta(T_{a\_dry}) + \gamma} f_e(u_2)\left[e_s(T_{a\_dry}) - e_{a\_dry}\right] \tag{16}$$

where e_{a_dry}, T_{a_dry}, and R_{n_dry} are e_a, T_a, and R_n under extremely dry conditions, respectively.

Here, we take RH = 10% to represent the RH of the atmosphere under the driest condition (RH$_{dry}$), which corresponds to the 0.1th percentile of the ERA5 monthly RH across all months from 1982 to 2011 over the entire terrestrial surfaces (Figure S2 in Supporting Information S1). Since RH is a relative measure while e_a is an absolute measure, it is more appropriate to use RH to define a single driest atmospheric humidity across the entire terrestrial environment to account for the impact of temperature difference on e_a.

Then, the atmospheric vapor pressure and air temperature corresponding to RH$_{dry}$ can be obtained by simultaneously solving the following equations within the constraint of an adiabatic process (Monteith, 1981),

$$\begin{cases} \mathrm{RH}_{dry} = \dfrac{e_{a\_dry}}{e_{s\_dry}(T_{a\_dry})} \\ -\gamma = \dfrac{e_a - e_{a\_dry}}{T_a - T_{a\_dry}} \end{cases} \tag{17}$$

To estimate R_n under the driest conditions, it is reasonable to assume that shortwave radiation remains unchanged as the shortwave radiation is largely independent of temperature and moisture (Yang & Roderick, 2019). Taking shortwave radiation unchanged also conforms with Brutsaert's (2015) idea of potential evaporation as having the same net solar radiative input as under real conditions. The net longwave radiation under the driest conditions can be estimated using an empirical equation recommended by the FAO (Allen et al., 1998),

$$R_{ln\_dry} = -\sigma T_{a\_dry}{}^4\left(0.34 - 0.14\sqrt{e_{a\_dry}}\right)(1.35 R_{si}/R_{si\_clear} - 0.35) \tag{18}$$

where R_{si} is the incoming shortwave radiation and R_{si_clear} is the clear-sky shortwave radiation. Note that under extremely dry conditions, R_{si} should approach R_{si_clear} and therefore the ratio of R_{si} over R_{si_clear} will approach 1.

4.2. Estimates of E_{pa_max}

In addition to E_{po}, the estimation of E_{pa_max} represents another key difference between the CR model developed above and that of Szilagyi et al. (2017). Hence, here, we first illustrate the estimates of E_{pa_max} and compare our estimates with that from Szilagyi et al. (2017). With E_{pa_max} derived from Equations 16–18, Figure 5a shows the spatial pattern of mean annual E_{pa_max}/E_{pa} at the 705 catchments and 64 flux sites. Because E_{pa_max} represents the highest E_{pa} under extremely dry conditions, the magnitudes of E_{pa_max}/E_{pa} should be all larger than 1. Our results show that the value of E_{pa_max}/E_{pa} is generally smaller than 1 in relatively dry regions and close to 1 in arid regions (e.g., the western US, southern Europe and western Australia), suggesting that the real climates in these regions are very close to their driest conditions. Conversely, larger E_{pa_max}/E_{pa} are found in relatively wet regions (e.g.,
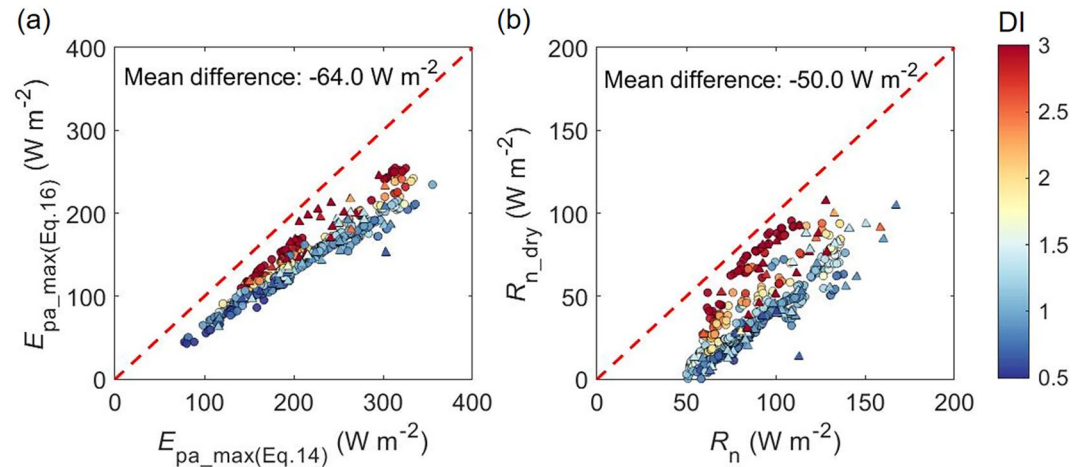
Figure 6. Comparison between (a) the estimated E_{pa_max} following Szilagyi et al. (2017) using Equations 14 and 15 (referred to $E_{pa\_max(Equation\ 14)}$) and the estimated E_{pa_max} with Equations 16–18 (referred to as $E_{pa\_max(Equation\ 16)}$), (b) the observed R_n directly used in Szilagyi et al. (2017) and the retrieved R_{n_dry} corresponding to the driest conditions in catchments (circle) and flux sites (triangle) at the mean annual scale. The dashed red line is the 1:1 line. Colors represent the dryness index (DI).

eastern US, Amazonia, and northern Europe in Figure 5a; DI < 1 in Figure 5b) and can exceed 2 in some high latitude cold, wet regions, indicating that E_{pa} under real conditions is at least two times smaller than the possible highest E_{pa} when the surface is totally dried out in these regions. The relationship between E_{pa_max}/E_{pa} and DI again confirms that E_{pa_max} is increasingly larger than E_{pa} as the climate becomes wetter and the value of E_{pa_max}/E_{pa} approaches 1 in extremely dry regions (Figure 5b).

Figure 6a shows the comparison between the E_{pa_max} estimated with the approach of Szilagyi et al. (2017) (Equations 14 and 15; referred to $E_{pa\_max(Equation\ 14)}$) and that estimated with the approach developed in this study (Equations 16–18; referred to as $E_{pa\_max(Equation\ 16)}$) for catchments and flux sites at the mean annual scale. The mean value of $E_{pa\_max(Equation\ 14)}$ is 64 W m^{-2} higher than $E_{pa\_max(Equation\ 16)}$, which is mainly caused by the higher R_n under real conditions compared with R_{n_dry} under hypothetical extremely dry conditions (Figure 6b). Our results show that when the actual climate is dry (DI > 2.5), the difference between R_n and R_{n_dry} is relatively small, leading to subtle differences between the two E_{pa_max} estimates. However, with the climate becoming wetter, our approach that considers the coupling between radiation and temperature yields a much lower R_{n_dry} than observed R_n and consequently a much lower $E_{pa\_max(Equation\ 16)}$ than $E_{pa\_max(Equation\ 14)}$.

4.3. Validation of the New CR Model

We next employ E_{po_max} estimated from the maximum evaporation method in the new CR (Equations 11, 12 and 16) to estimate E in 705 catchments at the mean annual scale, as well as at 64 flux sites at monthly and mean annual scales. For catchments, compared with E derived from catchment water balance at the mean annual scale, the estimated E has an R^2 of 0.73, a root-mean-squared error (RMSE) of 9.8 W m^{-2} and a mean bias (estimated mean minus observed mean) of 3.3 W m^{-2} (Figure 7). At flux sites, the estimated E shows an $R^2 = 0.74$, RMSE = 18.8 W m^{-2} and mean bias = -2.8 W m^{-2} at the monthly scale (Figure 8a) and an $R^2 = 0.75$, RMSE = 11.2 W m^{-2} and mean bias = -3.1 W m^{-2} at the mean annual scale (Figure 8b). The above results demonstrate the overall good performance of the new CR model in estimating E across catchments at the mean annual scale and at flux sites at both monthly and mean annual scales.

5. Discussion

The CR provides a simple framework for estimating actual evaporation with basic meteorological observations. Over the years, the complementarity
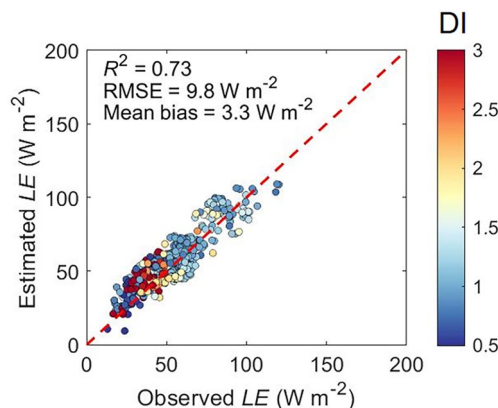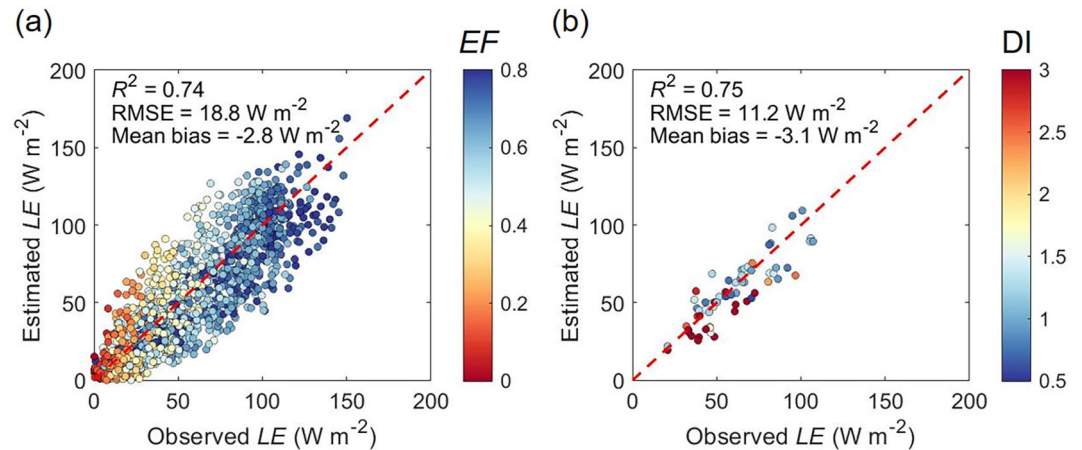

Figure 7. Validation of estimated E in the 705 catchments at the mean annual scale. The dashed red line is the 1:1 line. Colors represent the dryness index (DI).

Figure 8. Validation of estimated E at the 64 flux sites at (a) monthly scale, (b) mean annual scale. The dashed red line is the 1:1 line. Colors represent the evaporative fraction (EF) in panel (a) and dryness index (DI) in panel (b).

principle has evolved from a conceptual symmetric linear relationship (Bouchet, 1963) to a generalized asymmetric nonlinear relationship (Brutsaert, 2015; Brutsaert et al., 2020; S. Han & Tian, 2018; S. Han et al., 2021; Kim & Chun, 2021; Ma et al., 2021; Szilagyi et al., 2017). Nevertheless, the state-of-the-art CR models still suffer from two main issues. First, as a key variable in the CR, E_{po} estimates departure from its original definition which hinders the proper interpretation and understanding of the CR. According to its definition, E_{po} is "*the evaporation that takes place from the same surface as the actual evaporation when the evaporating water is not a limiting factor and with the same solar radiative input*" (Brutsaert, 2015). However, E_{po} estimated from conventional models (e.g., the Priestley-Taylor model, which is most widely used in CR models) often do not conform to its definition (Aminzadeh et al., 2016; Z. Liu & Yang, 2021; Z. Liu et al., 2022; Szilagyi & Jozsa, 2008; Tu & Yang, 2022; Yang & Roderick, 2019), as the observed meteorological variables under real conditions do not necessarily represent the forcings when the underlying surface is "hypothetically" non-water-limited (Figure 3; Tu & Yang, 2022). Second, most CR models contain model parameters that do not have a clear physical meaning and require local calibration. Although efforts have been made to develop empirical relationships between model parameters and environmental variables (Brutsaert et al., 2020; Gao & Xu, 2021; X. Liu et al., 2018; L. Wang et al., 2020, 2022), these empirical relationships only provide "physical connections" between the model parameters and environmental variables and cannot be used to interpret the physical meanings of these model parameters. In addition, extrapolating these empirical relationships beyond the places and periods of calibration may incur additional uncertainties in the model predictions.

The new CR model developed herein addresses these two fundamental issues. For the estimation of E_{po}, we adopt the maximum evaporation approach that explicitly acknowledges the interdependence between evaporation, surface temperature and radiation over wet surfaces. This enables both radiation and surface temperature to be recovered to a hypothetical wet condition (Tu et al., 2022; Yang & Roderick, 2019) such that the calculated E_{po} (i.e., E_{po_max}) closely follows the E_{po} definition (Tu & Yang, 2022). With E_{po_max} restored to a hypothetical wet (i.e., potential) condition, we develop a new CR model based on the generalized polynomial function of Brutsaert (2015) and the modified boundary condition under extremely dry conditions of Szilagyi et al. (2017). To address the issue of decoupled R_n and T_s in the estimation of E_{pa_max} in the approach of Szilagyi et al. (2017), we propose a physically based method to estimate E_{pa_max}, in which the interdependence between R_n and T_s is fully accounted (see Section 4.1). The fact that the new CR model does not require local calibration indicates it may be more suitable for predicting E in ungauged basins. This physically based CR model was validated and found to have an overall adequate performance in estimating actual evaporation in 705 catchments at the mean annual scale and across 64 flux sites at monthly and mean annual scales (Figures 7 and 8). In Supporting Information S1, we also compare the performance of the new CR model with three mainstream generalized CR models developed previously (Brutsaert, 2015; S. Han & Tian, 2018; Szilagyi et al., 2017; see Text S1 in Supporting Information S1 for details). Our comparison results show that the new CR model developed herein generally outperforms (or at least shows a similar performance with) those three mainstream generalized CR models at both catchments and flux sites (Figure S3 in Supporting Information S1).
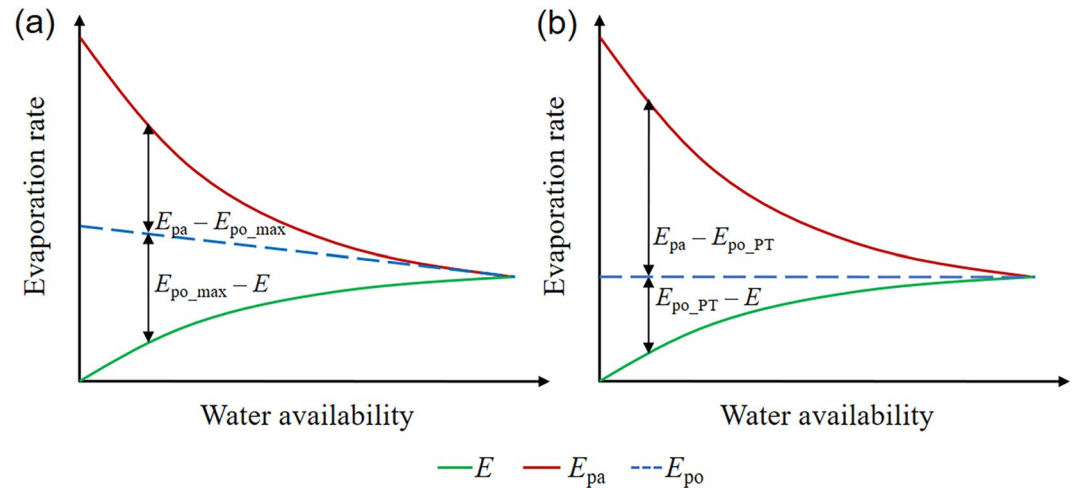
Figure 9. Conceptual plot of the complementary relationship (CR). Panel (a) shows the conceptual plot of the CR with E_{po} recovered to hypothetical saturated conditions (i.e., E_{po_max}). In comparison, panel (b) shows the conceptual plot of the CR with E_{po} calculated using conventional approaches (e.g., the Priestley-Taylor model forced with meteorological variables under real conditions, E_{po_PT}).

In addition to a better performance of estimating actual E, the adoption of E_{po_max} also has important implications in the interpretation of the CR. In existing CR approaches where E_{po} is calculated using fixed R_n (e.g., using the Priestley-Taylor approach), the interpretation of the CR is that as E increases with the increase of water supply, the air above the evaporating surface would become cooler and wetter, which leads to a decreased VPD and thus a decreased E_{pa}. The result of this interpretation is that both E and E_{pa} are complementary around a horizontal line of E_{po} across the entire moisture gradient (i.e., Figure 9b). However, E_{po} cannot remain unchanged with changing moisture availability. For the same net solar radiation, a drier (wetter) surface usually corresponds to a lower (higher) E and a higher (lower) surface temperature that directly leads to a larger (smaller) emitted longwave radiation and thus a lower (higher) R_n (Figure 3). This intrinsic physical interdependence between R_n, E, and T_s is ignored in the conventional E_{po} models but forms the basis of the maximum evaporation approach (Yang & Roderick, 2019). Compared with the Priestley-Taylor estimates, E_{po_max} is increasingly larger as the surface becomes drier, which is primarily caused by a higher R_n when restoring a dry surface to a hypothetical wet condition. This means that E and E_{pa} are not complementary around a fixed E_{po} but instead complementary around a decreasing E_{po} as the surface gets wetter (i.e., Figure 9a). A direct consequence of the higher E_{po} is that it effectively reduces the value of E_{pa}/E_{po} at the drier end, making the CR much less asymmetric than previously reported (Figure 4). In addition, since R_n also changes with surface wetting/drying, the interpretation of the CR should be modified to acknowledge this point. Here, we provide a new interpretation of the CR: as the underlying surface becomes wetter, a higher E leads to a cooler and wetter atmosphere and therefore a lower E_{pa}. Concurrently, a higher E results in a lower surface temperature that increases the net available energy of the surface, which simultaneously increases E_{pa} and E. The fact that E_{pa} still shows a decreasing trend from dry to wet conditions indicates that the decrease of E_{pa} induced by decreased VPD outweighs the increase of E_{pa} induced by increased R_n as the surface gets wetter.

Finally, it is worthwhile noting a few uncertainties/limitations in the current study. First, in the estimation of E_{pa_max}, we set a global value of RH$_{dry}$ as 10%, which corresponds to the 0.1th percentile of the global terrestrial 0.25° RH over all months during 1982–2011 in the ERA5 data set (Figure S2 in Supporting Information S1). To examine the uncertainties caused by adopting this value, we conducted an additional test that shows the model performance remains more or less unchanged for a RH$_{dry}$ range between 7% and 13% (Figure S4 in Supporting Information S1). Second, a previous study (S. Han & Tian, 2021) pointed out that the rescaling approach proposed by Szilagyi et al. (2017) and adopted herein may reduce the performance of the CR model when the estimated E_{po}/E_{pa} is smaller than its counterparts calculated from the cubic equation (Equation 10), as the scaling factor (i.e., $(E_{pa\_max} - E_{pa})/(E_{pa\_max} - E_{po})$) is always smaller than one and thus would move the point of E_{po}/E_{pa} to further away from the target point on the cubic curve. This issue often occurs when E_{po} is estimated using conventional E_{po} models (e.g., the Priestley-Taylor model; R. D. Crago & Qualls, 2018). Nevertheless, the issue

is largely avoided in the CR model developed here, as the maximum evaporation approach usually produces a larger E_{po} than conventional E_{po} models and the situation of smaller E_{po}/E_{pa} estimates than its counterparts calculated from the cubic equation is less likely to occur (Figure S5 in Supporting Information S1). Third, previous studies suggest that the CR would perform quite differently at different time scales (R. D. Crago et al., 2022; Morton, 1983; Szilagyi, 2021; L. Wang et al., 2021). Here, we only test the model performance at monthly and mean annual scales and find that the model performance slightly improved over the longer mean annual time scale (Figure 8). This suggests that applying the CR principle at shorter time scales (e.g., daily or sub-daily) may be more challenging, as it takes time for the vapor balance between the land and the atmosphere to be achieved. Testing the model performance over shorter time scales (e.g., daily or sub-daily) remains a high priority for future research.

6. Conclusion

In this study, we employed the maximum evaporation method to estimate E_{po} with T_s and R_n recovered to hypothetical wet conditions in the CR. Compared with the Priestley-Taylor model that has been most widely used in earlier CR models to estimate E_{po}, the restored lower T_s and higher R_n under non-saturated conditions lead to higher E_{po} estimates from the maximum evaporation approach (i.e., E_{po_max}). In addition, we find that adopting E_{po_max} considerably reduces the asymmetry of the complementarity between E/E_{po_max} and E_{pa}/E_{po_max} compared with existing studies. We then postulated a new, physically based, calibration-free CR model for estimating actual evaporation, based on the generalized polynomial function and a modified dry boundary condition, with the key variable required in the latter (i.e., E_{pa_max}) estimated from a full consideration of the interactions between R_n and T_s. This physically based CR model was validated to have an overall good performance in estimating actual evaporation in 705 catchments at the mean annual scale and across 64 flux sites at monthly and mean annual scales. More importantly, recovering E_{po} corresponding to its physical consideration provides new insights into the interpretation and understanding of the CR.

Conflict of Interest

The authors declare no conflicts of interest relevant to this study.

Data Availability Statement

The FLUXNET data were acquired from https://fluxnet.org/data/fluxnet2015-dataset/ (Pastorello et al., 2020). The ERA5 global reanalysis data were downloaded from the Copernicus Climate Change Service Climate Data Store (https://doi.org/10.24381/cds.f17050d7; Hersbach et al., 2020). Observed streamflow data were compiled from six sources including: (a) Global River Discharge Centre (http://www.bafg.de/GRDC; Lehner, 2012); (b) the U.S. Geological Survey (USGS) National Water Information System (https://waterdata.usgs.gov/nwis) and GAGES-II database (Falcone et al., 2010); (c) the Australian Bureau of Meteorology (http://www.bom.gov.au/waterdata; Y. Zhang et al., 2013); (d) the Brazilian Agência Nacional de Águas (http://www.snirh.gov.br/hidroweb); (e) the Water Survey of Canada Hydrometric Data (https://www.canada.ca/en/environment-climate-change); and (f) the Chilean Center for Climate and Resilience Research (http://www.cr2.cl/datos-de-caudales/).

References

Allen, R. G., Pereira, L. S., Raes, D., & Smith, M. (1998). *Crop evapotranspiration – Guidelines for computing crop water requirements – FAO Irrigation and drainage paper 56*. Food and Agriculture Organization.

Aminzadeh, M., Roderick, M. L., & Or, D. (2016). A generalized complementary relationship between actual and potential evaporation defined by a reference surface temperature. *Water Resources Research*, 52(1), 385–406. https://doi.org/10.1002/2015WR017969

Beck, H. E., Wood, E. F., McVicar, T. R., Zambrano-Bigiarini, M., Alvarez-Garreton, C., Baez-Villanueva, O. M., et al. (2020). Bias correction of global high-resolution precipitation climatologies using streamflow observations from 9372 catchments. *Journal of Climate*, 33(4), 1299–1315. https://doi.org/10.1175/JCLI-D-19-0332.1

Bouchet, R. (1963). Evapotranspiration reelle at potentielle, signification climatique. *IAHS Publication*, 62, 134–142. (in French).

Brutsaert, W. (1982). *Evaporation into the atmosphere: Theory, history and applications*. Springer Science & Business Media.

Brutsaert, W. (2005). *Hydrology: An introduction*. Cambridge University Press.

Brutsaert, W. (2015). A generalized complementary principle with physical constraints for land-surface evaporation. *Water Resources Research*, 51(10), 8087–8093. https://doi.org/10.1002/2015WR017720

Brutsaert, W., Cheng, L., & Zhang, L. (2020). Spatial distribution of global landscape evaporation in the early twenty-first century by means of a generalized complementary approach. *Journal of Hydrometeorology*, 21(2), 287–298. https://doi.org/10.1175/JHM-D-19-0208.1

Brutsaert, W., & Parlange, M. B. (1998). Hydrologic cycle explains the evaporation paradox. *Nature*, *396*(5), 300. https://doi.org/10.1038/23845

Brutsaert, W., & Stricker, H. (1979). Advection-aridity approach to estimate actual regional evapotranspiration. *Water Resources Research*, *15*(2), 443–450. https://doi.org/10.1029/WR015i002p00443

Crago, R., Szilagyi, J., Qualls, R., & Huntington, J. (2016). Rescaling the complementary relationship for land surface evaporation. *Water Resources Research*, *52*(11), 8461–8471. https://doi.org/10.1002/2016WR019753

Crago, R. D., Qualls, R., & Szilagyi, J. (2022). Complementary Relationship for evaporation performance at different spatial and temporal scales. *Journal of Hydrology*, *608*, 127575. https://doi.org/10.1016/j.jhydrol.2022.127575

Crago, R. D., & Qualls, R. J. (2018). Evaluation of the generalized and rescaled complementary evaporation relationships. *Water Resources Research*, *54*(10), 8086–8102. https://doi.org/10.1029/2018WR023401

Crago, R. D., & Qualls, R. J. (2021). A graphical interpretation of the rescaled complementary relationship for evapotranspiration. *Water Resources Research*, *57*(8), e2020WR028299. https://doi.org/10.1029/2020WR028299

Ershadi, A., McCabe, M. F., Evans, J. P., Chaney, N. W., & Wood, E. F. (2014). Multi-site evaluation of terrestrial evaporation models using FLUXNET data. *Agricultural and Forest Meteorology*, *187*, 46–61. https://doi.org/10.1016/j.agrformet.2013.11.008

Falcone, J. A., Carlisle, D. M., Wolock, D. M., & Meador, M. R. (2010). Gages: A stream gage database for evaluating natural and altered flow conditions in the conterminous United States [Dataset]. Ecology, *91*(2), 621. https://doi.org/10.1890/09-0889.1

Gao, B., & Xu, X. (2021). Derivation of an exponential complementary function with physical constraints for land surface evaporation estimation. *Journal of Hydrology*, *593*, 125623. https://doi.org/10.1016/j.jhydrol.2020.125623

Granger, R. J. (1989). A complementary relationship approach for evaporation from nonsaturated surfaces. *Journal of Hydrology*, *111*(1–4), 31–38. https://doi.org/10.1016/0022-1694(89)90250-3

Green, J. K., Seneviratne, S. I., Berg, A. M., Findell, K. L., Hagemann, S., Lawrence, D. M., & Gentine, P. (2019). Large influence of soil moisture on long-term terrestrial carbon uptake. *Nature*, *565*(7740), 476–479. https://doi.org/10.1038/s41586-018-0848-x

Han, J., Yang, Y., Roderick, M. L., McVicar, T. R., Yang, D., Zhang, S., & Beck, H. E. (2020). Assessing the steady-state assumption in water balance calculation across global catchments. *Water Resources Research*, *56*(7), e2020WR027392. https://doi.org/10.1029/2020WR027392

Han, S., Hu, H., & Tian, F. (2012). A nonlinear function approach for the normalized complementary relationship evaporation model. *Hydrological Processes*, *26*(26), 3973–3981. https://doi.org/10.1002/hyp.8414

Han, S., & Tian, F. (2018). Derivation of a sigmoid generalized complementary function for evaporation with physical constraints. *Water Resources Research*, *54*(7), 5050–5068. https://doi.org/10.1029/2017WR021755

Han, S., & Tian, F. (2020). A review of the complementary principle of evaporation: From the original linear relationship to generalized nonlinear functions. *Hydrology and Earth System Sciences*, *24*(5), 2269–2285. https://doi.org/10.5194/hess-24-2269-2020

Han, S., & Tian, F. (2021). Comment on "A Calibration-Free Formulation of the Complementary Relationship of Evaporation for Continental-Scale Hydrology" by J. Szilagyi et al. *Journal of Geophysical Research: Atmospheres*, *126*(9), e2020JD033403. https://doi.org/10.1029/2020JD033403

Han, S., Tian, F., Wang, W., & Wang, L. (2021). Sigmoid generalized complementary equation for evaporation over wet surfaces: A nonlinear modification of the Priestley-Taylor equation. *Water Resources Research*, *57*(9), e2020WR028737. https://doi.org/10.1029/2020WR028737

Hersbach, H., Bell, B., Berrisford, P., Hirahara, S., Horányi, A., Muñoz-Sabater, J., et al. (2020). The ERA5 global reanalysis [Dataset]. Quarterly Journal of the Royal Meteorological Society, *146*(730), 1999–2049. https://doi.org/10.1002/qj.3803

Kahler, D. M., & Brutsaert, W. (2006). Complementary relationship between daily evaporation in the environment and pan evaporation. *Water Resources Research*, *42*(5), W05413. https://doi.org/10.1029/2005WR004541

Kim, D., & Chun, J. A. (2021). Revisiting a two-parameter Budyko equation with the complementary evaporation principle for proper consideration of surface energy balance. *Water Resources Research*, *57*(11), e2021WR030838. https://doi.org/10.1029/2021WR030838

Lehner, B. (2012). Derivation of watershed boundaries for GRDC gauging stations based on the HydroSHEDS drainage network (Technical Report no. 41): Global Runoff Data Centre (GRDC) [Dataset]. Federal Institute of Hydrology (BfG). Retrieved from https://www.bafg.de/GRDC/EN/02_srvcs/24_rprtsrs/report_41.pdf?__blob=publicationFile

Liu, X., Liu, C., & Brutsaert, W. (2016). Regional evaporation estimates in the eastern monsoon region of China: Assessment of a nonlinear formulation of the complementary principle. *Water Resources Research*, *52*(12), 9511–9521. https://doi.org/10.1002/2016WR019340

Liu, X., Liu, C., & Brutsaert, W. (2018). Investigation of a generalized nonlinear form of the complementary principle for evaporation estimation. *Journal of Geophysical Research: Atmospheres*, *123*(8), 3933–3942. https://doi.org/10.1002/2017JD028035

Liu, Z., Han, J., & Yang, H. (2022). Assessing the ability of potential evaporation models to capture the sensitivity to temperature. *Agricultural and Forest Meteorology*, *317*, 108886. https://doi.org/10.1016/j.agrformet.2022.108886

Liu, Z., & Yang, H. (2021). Estimation of water surface energy partitioning with a conceptual atmospheric boundary layer model. *Geophysical Research Letters*, *48*(9), e2021GL092643. https://doi.org/10.1029/2021GL092643

Ma, N., Szilagyi, J., & Zhang, Y. (2021). Calibration-free complementary relationship estimates terrestrial evapotranspiration globally. *Water Resources Research*, *57*(9), e2021WR029691. https://doi.org/10.1029/2021WR029691

Ma, N., Szilagyi, J., Zhang, Y., & Liu, W. (2019). Complementary-relationship-based modeling of terrestrial evapotranspiration across China during 1982–2012: Validations and spatiotemporal analyses. *Journal of Geophysical Research: Atmospheres*, *124*(8), 4326–4351. https://doi.org/10.1029/2018JD029850

McMahon, T. A., Peel, M. C., Lowe, L., Srikanthan, R., & McVicar, T. R. (2013). Estimating actual, potential, reference crop and pan evaporation using standard meteorological data: A pragmatic synthesis. *Hydrology and Earth System Sciences*, *17*(4), 1331–1363. https://doi.org/10.5194/hess-17-1331-2013

Milly, P. C., & Dunne, K. A. (2016). Potential evapotranspiration and continental drying. *Nature Climate Change*, *6*(10), 946–949. https://doi.org/10.1038/nclimate3046

Monteith, J. L. (1981). Evaporation and surface temperature. *Quarterly Journal of the Royal Meteorological Society*, *107*(451), 1–27. https://doi.org/10.1002/qj.49710745102

Morton, F. I. (1983). Operational estimates of areal evapotranspiration and their significance to the science and practice of hydrology. *Journal of Hydrology*, *66*(1–4), 1–76. https://doi.org/10.1016/0022-1694(83)90177-4

Oki, T., & Kanae, S. (2006). Global hydrological cycles and world water resources. *Science*, *313*(5790), 1068–1072. https://doi.org/10.1126/science.1128845

Pastorello, G., Trotta, C., Canfora, E., Chu, H., Christianson, D., Cheah, Y. W., et al. (2020). The FLUXNET2015 dataset and the ONEFlux processing pipeline for eddy covariance data [Dataset]. Scientific Data, *7*(1), 1–27. https://doi.org/10.1038/s41597-020-0534-3

Penman, H. L. (1948). Natural evaporation from open water, bare soil and grass. *Proceedings of the Royal Society of London, Series A: Mathematical and Physical Sciences*, *193*(1032), 120–145. https://doi.org/10.1098/rspa.1948.0037

Philip, J. R. (1987). A physical bound on the Bowen ratio. *Journal of Climate and Applied Meteorolog*y, *26*(8), 1043–1045. https://doi.org/10.1175/1520-0450(1987)026<1043:apbotb>2.0.co;2

Priestley, C. H. B., & Taylor, R. J. (1972). On the assessment of surface heat flux and evaporation using large-scale parameters. *Monthly Weather Review*, *100*(2), 81–92. https://doi.org/10.1175/1520-0493(1972)100<0081:OTAOSH>2.3.CO;2

Qualls, R. J., & Crago, R. D. (2020). Graphical interpretation of wet surface evaporation equations. *Water Resources Research*, *56*(10), e2019WR026766. https://doi.org/10.1029/2019WR026766

Shuttleworth, W. J. (1993). Evaporation. In D. R. Maidment (Ed.), *Handbook of hydrolog*y (p. 1424). McGraw-Hill Education.

Szilagyi, J. (2007). On the inherent asymmetric nature of the complementary relationship of evaporation. *Geophysical Research Letters*, *34*(2), L02405. https://doi.org/10.1029/2006GL028708

Szilagyi, J. (2014). Temperature corrections in the Priestley–Taylor equation of evaporation. *Journal of Hydrology*, *519*, 455–464. https://doi.org/10.1016/j.jhydrol.2014.07.040

Szilagyi, J. (2021). On the thermodynamic foundations of the complementary relationship of evaporation. *Journal of Hydrology*, *593*, 125916. https://doi.org/10.1016/j.jhydrol.2020.125916

Szilagyi, J., Crago, R., & Qualls, R. (2017). A calibration-free formulation of the complementary relationship of evaporation for continental-scale hydrology. *Journal of Geophysical Research: Atmospheres*, *122*(1), 264–278. https://doi.org/10.1002/2016JD025611

Szilagyi, J., & Jozsa, J. (2008). New findings about the complementary relationship-based evaporation estimation methods. *Journal of Hydrology*, *354*(1–4), 171–186. https://doi.org/10.1016/j.jhydrol.2008.03.008

Szilagyi, J., Ma, N., Crago, R. D., & Qualls, R. J. (2022). Power-function expansion of the nondimensional complementary relationship of evaporation: The emergence of dual attractors. *Earth and Space Science Open Archive*. https://doi.org/10.1002/essoar.10510255.1

Szilagyi, J., & Schepers, A. (2014). Coupled heat and vapor transport: The thermostat effect of a freely evaporating land surface. *Geophysical Research Letters*, *41*(2), 435–441. https://doi.org/10.1002/2013GL058979

Trenberth, K. E., Fasullo, J. T., & Kiehl, J. (2009). Earth's global energy budget. *Bulletin of the American Meteorological Society*, *90*(3), 311–324. https://doi.org/10.1175/2008BAMS2634.1

Tu, Z., & Yang, Y. (2022). On the estimation of potential evaporation under wet and dry conditions. *Water Resources Research*, *58*(4), e2021WR031486. https://doi.org/10.1029/2021WR031486

Tu, Z., Yang, Y., & Roderick, M. L. (2022). Testing a maximum evaporation theory over saturated land: Implications for potential evaporation estimation. *Hydrology and Earth System Sciences*, *26*(7), 1745–1754. https://doi.org/10.5194/hess-26-1745-2022

Wang, K., & Dickinson, R. E. (2012). A review of global terrestrial evapotranspiration: Observation, modeling, climatology, and climatic variability. *Reviews of Geophysics*, *50*(2), RG2005. https://doi.org/10.1029/2011RG000373

Wang, L., Han, S., & Tian, F. (2021). At which timescale does the complementary principle perform best in evaporation estimation? *Hydrology and Earth System Sciences*, *25*(1), 375–386. https://doi.org/10.5194/hess-25-375-2021

Wang, L., Tian, F., Han, S., Cui, T., Meng, X., & Hu, H. (2022). Determination of the asymmetric parameter in complementary relations of evaporation in alpine grasslands of the Tibetan Plateau. *Journal of Hydrology*, *605*, 127306. https://doi.org/10.1016/j.jhydrol.2021.127306

Wang, L., Tian, F., Han, S., & Wei, Z. (2020). Determinants of the asymmetric parameter in the generalized complementary principle of evaporation. *Water Resources Research*, *56*(9), e2019WR026570. https://doi.org/10.1029/2019WR026570

Yang, Y., & Roderick, M. L. (2019). Radiation, surface temperature and evaporation over wet surfaces. *Quarterly Journal of the Royal Meteorological Society*, *145*(720), 1118–1129. https://doi.org/10.1002/qj.3481

Yang, Y., Roderick, M. L., Yang, D., Wang, Z., Ruan, F., McVicar, T. R., et al. (2021). Streamflow stationarity in a changing world. *Environmental Research Letters*, *16*(6), 064096. https://doi.org/10.1088/1748-9326/ac08c1

Yang, Y., Roderick, M. L., Zhang, S., McVicar, T. R., & Donohue, R. J. (2019). Hydrologic implications of vegetation response to elevated CO_2 in climate projections. *Nature Climate Change*, *9*(1), 44–48. https://doi.org/10.1038/s41558-018-0361-0

Zhang, L., & Brutsaert, W. (2021). Blending the evaporation precipitation ratio with the complementary principle function for the prediction of evaporation. *Water Resources Research*, *57*(7), e2021WR029729. https://doi.org/10.1029/2021WR029729

Zhang, L., Cheng, L., & Brutsaert, W. (2017). Estimation of land surface evaporation using a generalized nonlinear complementary relationship. *Journal of Geophysical Research: Atmospheres*, *122*(3), 1475–1487. https://doi.org/10.1002/2016JD025936

Zhang, Y., Viney, N., Frost, A., Oke, A., Brooks, M., Chen, Y., & Campbell, N. (2013). Collation of Australian modeller's streamflow dataset for 780 unregulated Australian catchments (Technical Report No. EP113194, p. 115) [Dataset]. CSIRO: Water for a Healthy Country National Research Flagship. Retrieved from https://publications.csiro.au/rpr/download?pid=csiro:EP113194&dsid=DS4

References From the Supporting Information

Beck, H. E., Zimmermann, N. E., McVicar, T. R., Vergopolan, N., Berg, A., & Wood, E. F. (2018). Present and future Köppen-Geiger climate classification maps at 1-km resolution. *Scientific Data*, *5*(1), 1–12. https://doi.org/10.1038/sdata.2018.214